Journal of Catalysis **203,** 351–361 (2001)
doi:10.1006/jcat.2001.3338, available online at http://www.idealibrary.com on IDEAL®

Applied Molecular Simulations over FER-, TON-, and AEL-Type Zeolites

L. Domokos,*,[1] L. Lefferts,* K. Seshan,* and J. A. Lercher†,[2]

*Faculty of Chemical Technology, University of Twente, PO Box 217, 7500 AE, The Netherlands; and †Institut für Technische Chemie, Technische Universität München, Lichtenbergstrasse 4, D-85748 Garching, Germany

Received February 13, 2001; revised June 28, 2001; accepted July 4, 2001

Interaction and transport of representative (un)saturated hydrocarbon molecules involved in the proposed reaction network of *n*-butene isomerization in zeolites FER, TON, and AEL have been studied by classic molecular modeling calculations. Docking of the guest molecules into the zeolite frameworks revealed that isomers up to eight carbon atoms can be located inside the pores without significant conformational restraints. FER and AEL zeolites showed higher stabilization compared with TON zeolites for di- and tribranched octanes proposed as intermediates for selective bimolecular mechanisms. Simulated diffusion profiles of such highly branched molecules showed large diffusion barriers, confirming their low uptake found in previous adsorption studies. Docking and diffusion calculations with coke precursors, such as benzene, naphthalene, and biphenyl, revealed that condensed ring structures are unlikely to be formed inside of the zeolite channels investigated. © 2001 Academic Press

Key Words: **skeletal isomerization; TON; AEL; molecular dynamics calculations; diffusion.**

1. INTRODUCTION

In the last two decades, molecular simulations, especially classic molecular modeling calculations, have matured into a widely accepted and implemented method and, in turn, have markedly improved the understanding of structure–property relationships in microporous materials at the molecular level. Classic molecular calculations, including molecular mechanics (MM) and molecular dynamics (MD), have gained widespread acceptance especially for large-scale systems, such as zeolites, while quantum mechanics (QM) calculations remained restricted to small clusters due to the greater computational requirements. State of the art "embedded"-type calculations showed that by involving part of the zeolite pore wall in the calculations, substantial changes occurred in potential energy and nonconventional species could be stabilized (1).

The understanding of the acid-catalyzed transformation of *n*-butene to isobutene on a molecular level represents a unique challenge. Three different mechanisms were proposed for the selective reaction: mono-, bi-, and pseudomonomolecular mechanisms (2–10). Exploring the viability of the monomolecular mechanism (2–4) attracted significant attention, since this mechanism proposes intermediates and a transition state that is energetically highly unfavorable. Therefore, large efforts have been taken to justify the existence of such intermediates and transition states in zeolites by using quantum mechanical methods (11, 12).

The bimolecular (5–7) and pseudomonomolecular mechanisms (8–10), however, offer energetically more favorable reaction pathways. Surprisingly, few systematic attempts have been reported to theoretically confirm the location and, essentially, the possible existence of the proposed intermediates of these mechanisms (5, 13). In principle, 10 member ring (MR) zeolites might constrain the formation of those bulky species, and thus drastically retard these reactions.

Skeletal isomerization is selective over some FER, TON, and AEL types of zeolites (14–19), all of them having monodimensional 10 MR channels, but the performance of the catalysts usually depends on rather subtle experimental details (17). It is thus important to examine the undisturbed effect of the ideal siliceous structure in the isomerization reaction, without effects such as acid site concentration (18), acid strength (19), and degree of crystallinity.

Configurational-bias Monte-Carlo (CB-MC) calculations are recognized as a powerful tool to estimate the heat of adsorption and other thermodynamic properties at fixed temperature and chemical potential in microporous materials (20). However, the approximation of replacing CH_3 and CH_2 groups in hydrocarbons with pseudoatoms represents a conceptual challenge in pore structures closely resembling the size of the adsorbate molecules. This is due to the fact that the nonspherically symmetric aliphatic groups and the atoms of the pore wall might be involved in an attractive interaction, while the spherical pseudoatoms might be rejected during the simulation because of the repulsive forces present due to significant overlapping.

[1] Current address: Shell Research and Technology Centre, Amsterdam, Badhuisweg 3, 1031 CM Amsterdam, The Netherlands.

[2] To whom correspondence should be addressed. Fax: 49-89-28913544. E-mail: johannes.lercher@ch.tum.de.

0021-9517/01 $35.00

Furthermore, the steric difference in the presence of a carbon–carbon double bond is neglected in these types of calculations. In addition, the intimate intramolecular interactions present in branched molecules cannot be modeled using equal sized pseudoatoms instead of aliphatic funcional groups. At last, it is known that by increasing the length of the chain, the projected molecular properties deviate from those measured in zeolites containing small pores (21, 22). This is because during calculation, the adsorbate is built from the pseudoatoms, and therefore, in confined spaces, the closely packed conformers are typically neglected in favor of the linear conformers (23). Consequently, the approach to the chemical representation of the adsorbate and the adsorbant might be more viable, and expected to lead to somewhat different results, especially at higher carbon numbers, which should therefore be carefully evaluated.

In this paper, the results of the docking and diffusion pathway methods of the InsightII program package from MSI are applied to a large selection of molecules typically observed during butene isomerization in the siliceous framework of FER-, TON-, and AEL-type zeolites. Comparison of host–guest interactions in the minimized structures, as well as the various diffusion pathways, is carried out. Implications to the previously proposed reaction mechanisms based on the divergences found regarding the zeolites structures are outlined.

2. COMPUTATIONAL DETAILS

2.1. Hydrocarbon Guest Molecules

Alkenes were used in the range between C_3 and C_7 molecules with linear or monobranched skeleton in both docking and diffusion calculations. For the C_8 molecules, due to the wide variety of skeletal and conformational isomers, only alkanes were used in the simulations. All enantiomers of the branched C_8 isomers were evaluated in the docking procedure (Fig. 1). This was required to evaluate the influence of the arrangement of the methyl groups on the sorption structures. Benzene, naphthalene, and ethylene-biphenyl were used to represent coke-type species. All molecules were optimized by means of energy minimization prior to calculations. Abbreviations for the different molecules used in the graphs are given in Table 1.

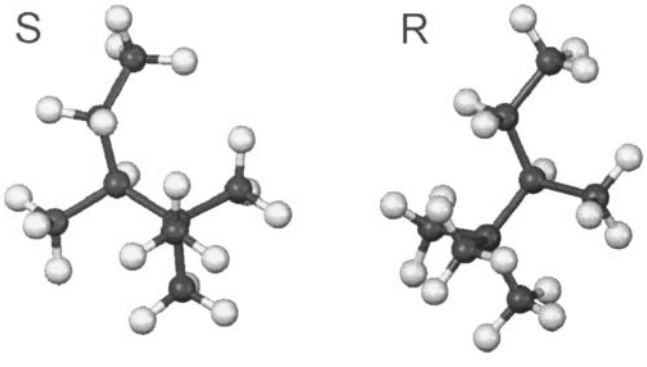

FIG. 1. Possible stereoisomers of a C_8 isomer. *S* and *R* isomers of 2,2,3-trimethylpentane are shown.

2.2. Zeolites

During docking calculations, hydrocarbon guests were fitted into the unit cell of the zeolite. To exclude the effect of cluster termination, periodic boundary conditions (PBC) were applied to the host structure. This allowed an infinite representation of the framework along the Cartesian coordinates. The zeolites were represented in all siliceous form, which eliminated the possible interactions of guest molecules with the acid sites. This is reasonable, since pore geometry was shown to contribute more to the adsorption enthalpy of alkanes compared with acid side concentration and strength for reactions over medium-pore zeolites (24). Furthermore, as was shown by Jousse *et al.* (25), the difference in interaction between acidic and nonacidic zeolites is almost entirely compensated by interaction via the molecular multipole moments and polarizability, which is not accounted for in the force field simulations. In the case of AEL zeolite, the all-silica framework exhibits a hypothetical structure, since originally this zeolite is an aluminophosphate. The approximation made by replacing aluminum and phosphorus with silicon is experimentally justified (26). Note that lattice parameters, such as pore dimensions and unit cell size, were kept identical to those of the original structure.

2.3. Force Field

In every calculation, the cff91_czeo force field was applied to estimate the interactions between the guest and host structures. This is based on the constant valence force field (cvff) and extended with the special hybridization states of silicon, oxygen, and aluminum found in zeolites. It is refined to match the interactions of hydrocarbons in zeolite framework measured by microcalorimetric and spectroscopic methods. Charges were not applied during calculations. Therefore, only the short-range dispersive interactions are estimated during simulation. Note that in the case of olefins, the interaction with acid sites is more significant due to additional nondispersive forces.

2.4. Computers and Software

Calculations were performed using the InsightII and Cerius^2 software package from Molecular Simulation Inc. Since all calculations required several distinct steps and theoretical methods, the following modules were used consecutively. Hydrocarbon molecules were constructed using the "Builder" module, zeolites (unit cells and clusters) were built using the "Solids Builder" module. This ensured the

TABLE 1

Lowest Total Energy of Cluster after Minimization of the Structures Resulting from the Docking Procedure

Name		Energy of cluster (kJ/mol)			
Guest molecule	IUPAC name	FER 8MR	FER 10MR	TON	AEL
Propene	Propene	−48	−33	−32	−41
But-1-ene	But-1-ene	−71	−52	−50	−65
Pent-1-ene	Pent-1-ene	−81	−68	−69	−84
Hex-1-ene	Hex-1-ene	−98	−83	−83	−105
Hept-1-ene	Hept-1-ene	−102	−99	−100	−118
t-2-Butene	(*E*)-But-2-ene	−54	−40	−38	−53
t-2-Pentene	(*E*)-Pent-2-ene	−67	−60	−55	−77
t-2-Hexene	(*E*)-Hex-2-ene	−85	−74	−71	−96
t-2-Heptene	(*E*)-Hept-2-ene	−95	−86	−82	−102
c-2-Butene	(*Z*)-But-2-ene	−54	−33	−32	−50
c-2-Pentene	(*Z*)-Pent-2-ene	−71	−55	−56	−75
c-2-Hexene	(*Z*)-Hex-2-ene	−78	−70	−69	−92
c-2-Heptene	(*Z*)-Hept-2-ene	−91	−82	−84	−101
Isobutene	Methylpropene	−51	−35	−39	−49
m2but1ene	2-Methylbut-1ene	−70	−55	−52	−71
m2pent1ene	2-Methylpent-1-ene	−81	−66	−68	−92
m2but2ene	2-Methylbut-2-ene	−51	−35	−33	−55
m2pent2ene	2-Methylpent-2-ene	−62	−55	−53	−80
22dmb	2,2-Dimethylbutane	−98	−76	−61	−74
22dmp	2,2-Dimethylpentane	−102	−88	−80	−103
22dmh	2,2-Dimethylhexane	−114	−102	−95	−115
24dmh_s	(*S*)-2,4-Dimethylhexane	−124	−110	−111	−128
24dmh_r	(*R*)-2,4-Dimethylhexane	−119	−111	−112	−132
34dmh_rs	(3*R*,4*S*)-3,4-Dimethylhexane	−115	−107	−86	−121
34dmh_ss	(3*S*,4*S*)-3,4-Dimethylhexane	−115	−105	−97	−122
23dmh_s	(*S*)-2,3-Dimethylhexane	−117	−105	−98	−104
23dmh_r	(*R*)-2,3-Dimethylhexane	−125	−108	−108	−110
224tmp	2,2,4-Trimethylpentane	−95	−87	−60	−92
234tmp	2,3,4-Trimethylpentane	−101	−92	−65	−90
223tmp_s	(*S*)-2,2,3-Trimethylpentane	−103	−84	−43	−78
223tmp_r	(*R*)-2,2,3-Trimethylpentane	−89	−89	−45	−76
Benzene	Benzene	−39	−16	−12	−35
Naphthalene	Naphthalene	401	407	409	380
Biphenyl	1,2-Diphenylethane	−71	−71	43	−42

use of well-reported crystallographic data. “Solids Docking” and “Solids Diffusion” modules were used to calculate docking of hydrocarbon guests in a zeolite unit cell (host) and the average energy barrier during diffusion of hydrocarbons in zeolite framework, respectively. Molecular modeling (MD) calculations (including the minimization of the hydrocarbons) were performed with the “Discover” module. More information on these procedures can be found in Ref. (27).

2.5. Solids Docking

With this method, interactions of guest molecules with a host structure were explored to simulate corresponding structural and thermodynamic data by locating preferred structural arrangements of guest molecules in the zeolite frameworks. The “Solids Docking” method uses a combination of Monte-Carlo and molecular mechanics techniques to probe preferred configurations of molecules within or in the close vicinity of a host structure (28). During calculations, high-temperature (1500 K) conformers of guest molecules were generated using the “Discover” package. This procedure is necessary to simulate flexible molecules, and it is performed to explore the conformational space of the sorbate. During the MD run, at least 50 molecules from the generated conformers were extracted randomly, and stored in a temporary file to be used in the following Monte-Carlo docking procedure (Fig. 2).

The obtained conformers were randomly placed into the zeolite cluster applying a maximum energy restriction to avoid overlapping atoms (Fig. 3). PBC were applied to simulate an infinite pore structure of the zeolite built from the corresponding unit cell representing an infinite dilution of the adsorbate. In a typical run, the level of intramolecular distortion in the guest molecule equaled the thermal energy at 1500 K (MD), while the interaction with the framework

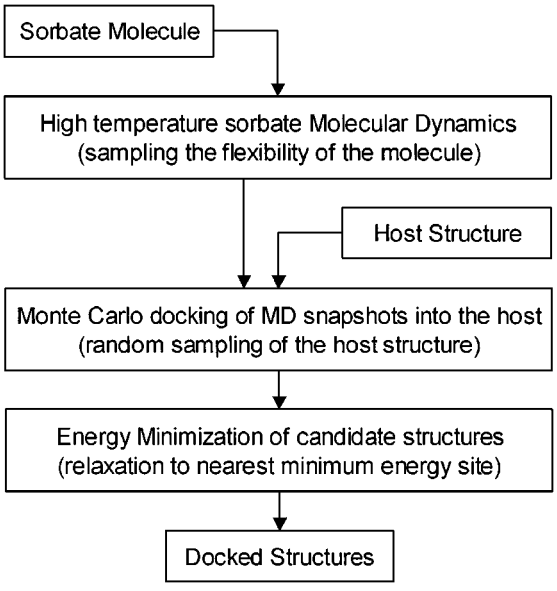

FIG. 2. Summary of the docking method (28).

did not exceed the acceptance level (typically 2000 kJ/mol) based on Lennard-Jones potentials. The acceptance level is set relatively high, since the Lennard-Jones potential is highly repulsive even at moderate steric overlaps. In practice, this steric hindrance was rapidly relieved during minimization.

The sets obtained from the Monte-Carlo docking procedure were relaxed in a zeolite cell using PBC. The zeolite lattice was kept fixed during the calculations. Constraints were not applied to the guest molecules, which allowed their migration to the local structural and energy minimum (Fig. 4).

Intra- and intermolecular interactions for host and guest were estimated by using the cff91_czeo force field. Since only dispersive (short-range) interactions were taken into account, a spherical cutoff at 15 Å was applied when guest–host interactions were calculated to reduce computational time.

2.6. Diffusion Pathway

With this method, a constrained minimization of a sorbate molecule, which is forced to move stepwise along a pathway fixed by multiple anchor points, was performed in the zeolite structures. This method in general enables quantitative evaluation of potential diffusion pathways (29). The anchor points consisted of nonframework pseudo or dummy atoms defined in the geometric center of the pore's cross section, giving a diffusion trajectory in the channel (Fig. 5).

The center of the guest molecule was constrained to a plane perpendicular to the defined trajectory by the anchor points at every step. With this restraint, greater rotational freedom was provided to the molecule inside the usually nonsymmetrical zeolite pores. Then, the structure was minimized and the intermolecular energy was evaluated. Optionally, in some cases molecular dynamics was performed to allow greater conformational sampling, although in most of the cases it did not add significantly to the result. Interaction between guest and host was estimated using the cff91_czeo forcefield. The conformation of the host–guest assembly was saved to an archive file at every step for later analysis.

During this type of calculation, the zeolite framework consisted of 10 unit cells in the direction of the diffusion pathway. The cross section of the simulation box was

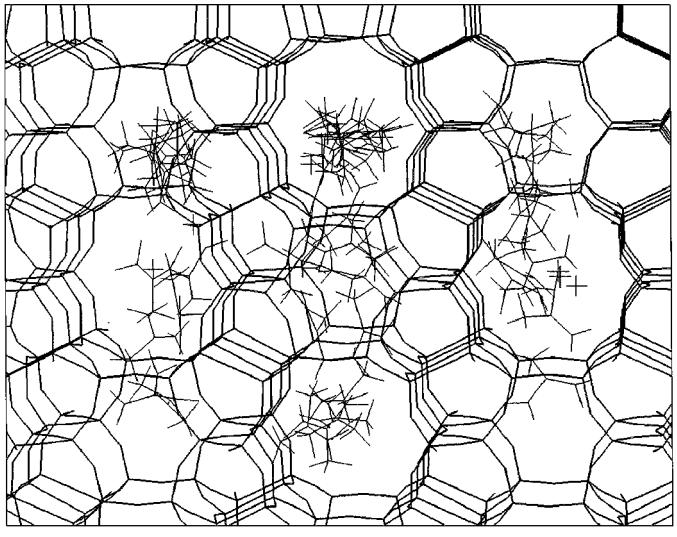

FIG. 3. Superimposed isobutene skeletons in FER prior to minimization. This view (along the 10 MR channels) reveals that a wide distribution of starting conformers are selected.

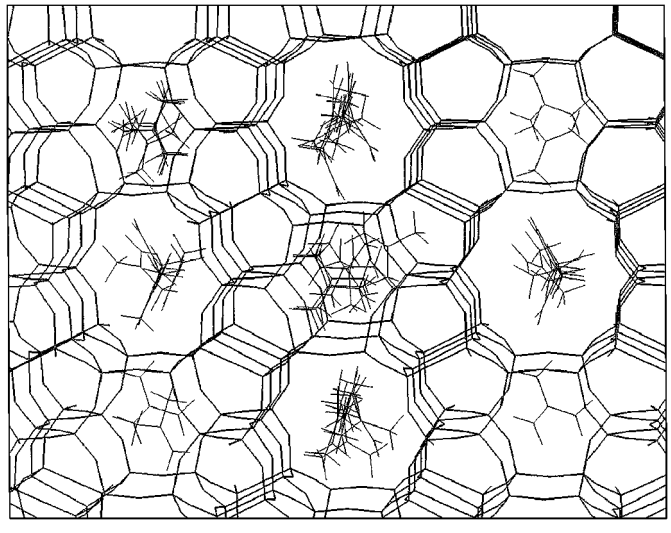

FIG. 4. View of Fig. 3 after minimization. It can be seen that similar docked structures can be achieved from different initial sets.

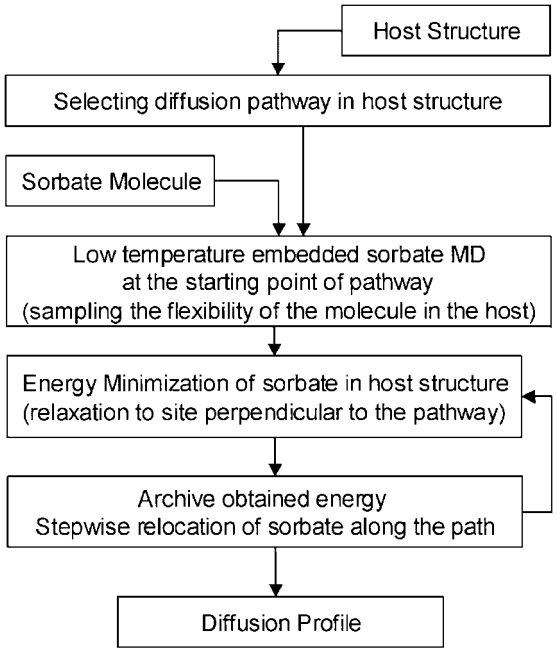

FIG. 5. Summary of the diffusion pathway method.

defined to be large enough to extend well over the cutoff radius (typically 15 Å) applied during the molecular dynamics calculations. This ensured full representation of the host structure and minimized computation time.

3. RESULTS

3.1. Docking of Hydrocarbons

The lowest total energies of the minimized clusters after docking are compiled in Table 1. For alkenes with a C_3–C_7 linear skeleton, these energies are plotted against the carbon number and presented in Fig. 6. A linear increase in energy was observed with all structures. The energies obtained with TON and the 10 MR in FER were very similar and exhibit a similar trend with increasing number of carbon atoms, while the energies obtained in the 8 MR of FER and in the elliptical 10-membered rings of AEL show different slopes. The change in the energies obtained in the 8 MR cages of FER is smaller compared with that obtained in the AEL structure.

Alkenes with a monobranched skeleton showed a similar trend in minimized docking energies with respect to increasing carbon numbers. The location of the double bond in the molecule, however, showed a clear influence on the minimal energy: the more rigid 2-methyl-2-butene and 2-methyl-2-pentene did not reach the minima of the corresponding 1-olefins (Fig. 7).

Octane isomers showed a less evident trend. It is important to note that all of them reached negative minima in every zeolite structure (Fig. 8). Moreover, dibranched isomers reached larger energy minima during the docking procedure compared with the tribranched isomers. In general, molecules in the 8 MR channels of FER reached lower energy levels compared with the 10 MR channels. Dibranched isomers reached similar docking energy in the 10 MR channels of FER and in TON, except (3*R*,4*S*)-3,4-dimethylhexane, which gained significantly less energy in TON. Dibranched isomers in general gained higher compensation in AEL compared with FER and TON, except for 2,3-dimethylhexane (both enantiomers), which showed similar energies in all catalysts.

Tribranched isomers showed lower stabilization in all the catalysts due to their more bulky structure, which tolerates less distortion and/or conformational changes required for docking in zeolites. Surprisingly, tribranched isomers reached significantly smaller energies in TON compared with FER and AEL. In FER and AEL similar energies were found, with the FER structure slightly favored.

The stabilization of dibranched and tribranched isomers compared results solely from the interaction of the hydrocarbon molecules and the oxygens of the pore wall. The flexibility of the alkane molecules ensured that repulsive forces are minimized, while attractive forces are maximized.

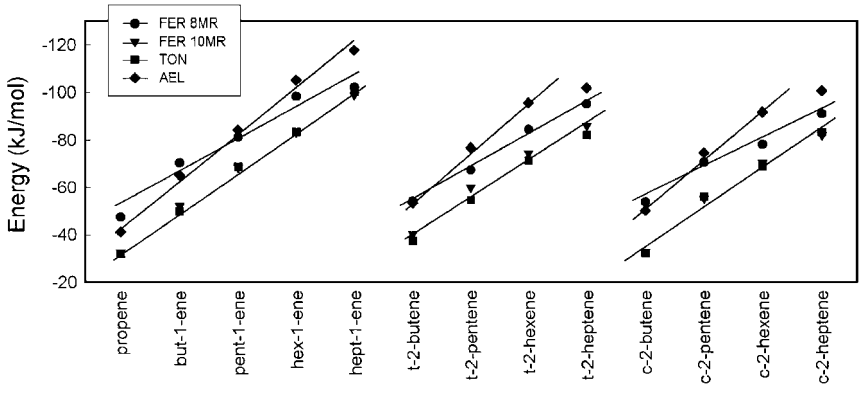

FIG. 6. Energy of cluster after minimization in FER-, TON-, and AEL-type zeolites versus carbon number in olefin isomers.

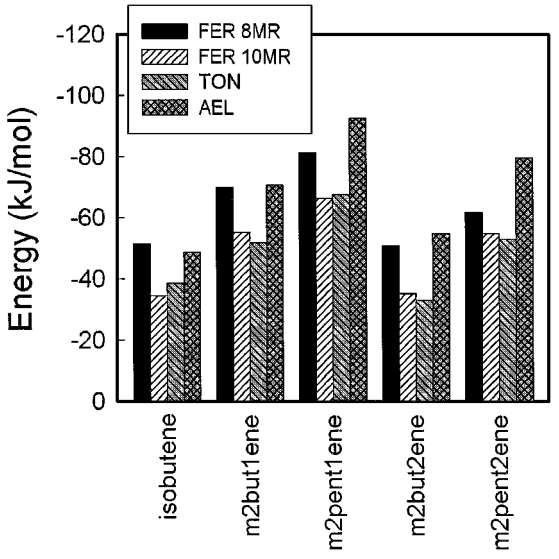

FIG. 7. Energy minimum of monobranched olefins in FER, TON, and AEL zeolites.

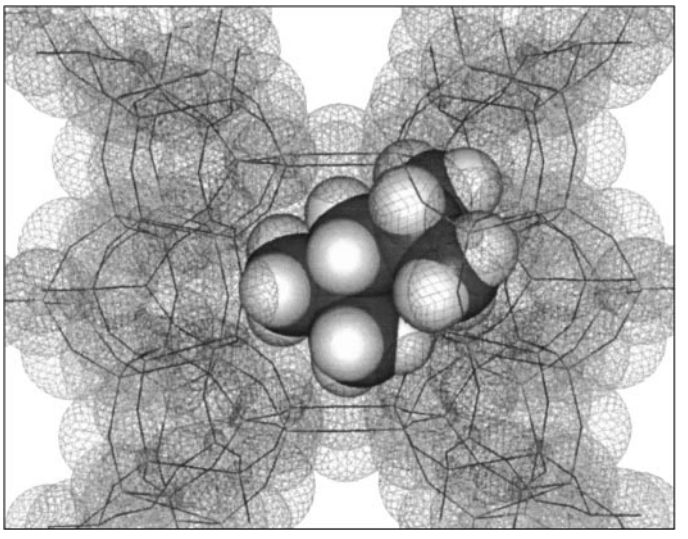

FIG. 9. Graphical representation of 2,2,4-trimethylpentane (guest) in FER (host). The guest is shown as CPK volume; the host, as a mesh model.

In Fig. 9 a stabilized 2,2,4-trimethylpentane is shown in the 8 MR cage of FER viewed along the [010] direction. The hydrocarbon molecule is represented as CPK; the zeolite framework is shown as a mesh model to increase the transparency of the structure. The molecule fits very well, as the interaction is maximized, and the gain from the attractive van der Waals forces results in a docking energy of approximately −95 kJ/mol for the cluster.

The docking energies obtained for aromatic species are depicted in Fig. 10. Benzene showed a modest energy gain in every structure, although higher gains were noted in 8 MR channels of FER and in AEL. 1,2-Biphenylethane reached lower energy in FER and in AEL, but showed positive energies in TON, indicating its unfavored existence in this structure. Naphthalene, a considerably more rigid molecule, showed large positive values for the minimized docking energies in every zeolite, clearly indicating that the repulsive forces resulting from the large overlap with the framework atoms could not be compensated by the attractive interactions, and made the minimized structures highly unfavorable irrespective of the structure of the zeolite. Note that in the case of naphthalene, the total potential energy is governed by the intramolecular torsion due to the very high rigidity of the molecule.

3.2. *Diffusion Pathway*

Typical energy profiles of isobutene and *trans*-2-butene translatory pathway obtained from "diffusion pathway" calculations are shown in Fig. 11. The difference between a minimum and maximum of the potential energy profile can be realized as the energy barrier the molecule overcomes during diffusion. Due to its larger kinetic diameter,

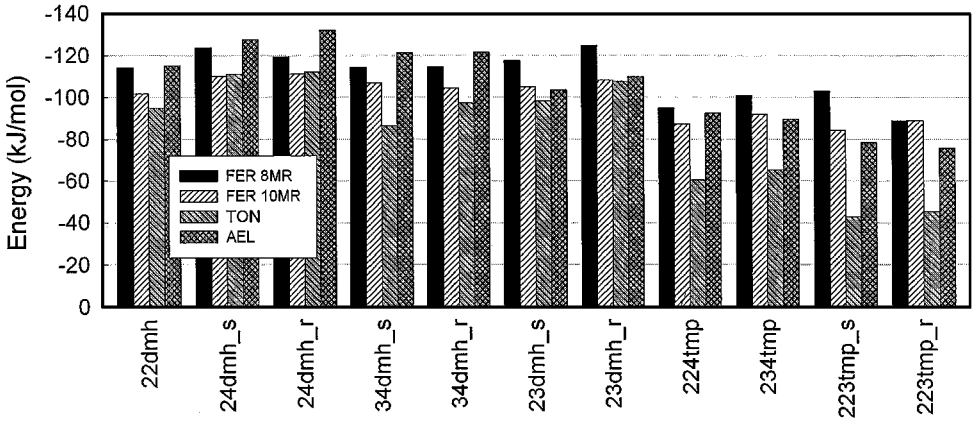

FIG. 8. Energy minimum reached by octane isomers in different zeolites.

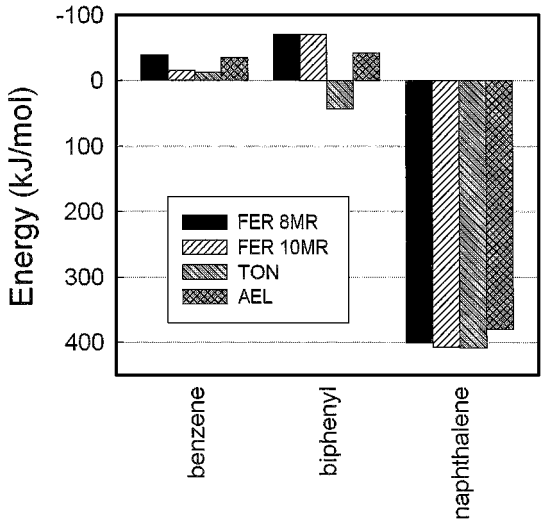

FIG. 10. Energy of aromatic species in FER, TON, and AEL.

isobutene showed a higher energy barrier in all zeolites compared with *trans*-2-butene. The energy barrier for isobutene diffusion was the highest along the 8 MR channels in FER due to the higher steric constraints in the narrow channels, while in TON and AEL, lower energy barriers were observed for isobutene.

The average energy barriers for *trans*-2-butene diffusion were very similar in the 10 MR channels of FER, TON, and AEL. In line with expectations, along the 8 MR channels, higher energy barriers were observed. In general, significantly higher energy barriers were calculated for all molecules in this direction due to the large repulsion caused by moving the guest molecule across the window of the 8 MR cages (Fig. 12).

The shape of the pore led to significant differences in energy barriers of molecules with increasing geometric cross section. By increasing the size of the window from 8 MR to 10 MR, the average energy barrier dropped approximately one order of magnitude. FER showed the highest energy barrier for all molecules. In the case of molecules with an elongated cross section the more elliptical shape of the pores in TON and AEL helped to decrease the overall energy barriers during diffusion. The exceptions are 2,2,4-trimethylpentane and 1,2-biphenylethane, which had a higher energy barrier in AEL as molecules with a bulkier cross section experience more repulsion in the narrow elliptical channels. In general, C_8 isomers with higher degree of branching showed higher barriers in every zeolite.

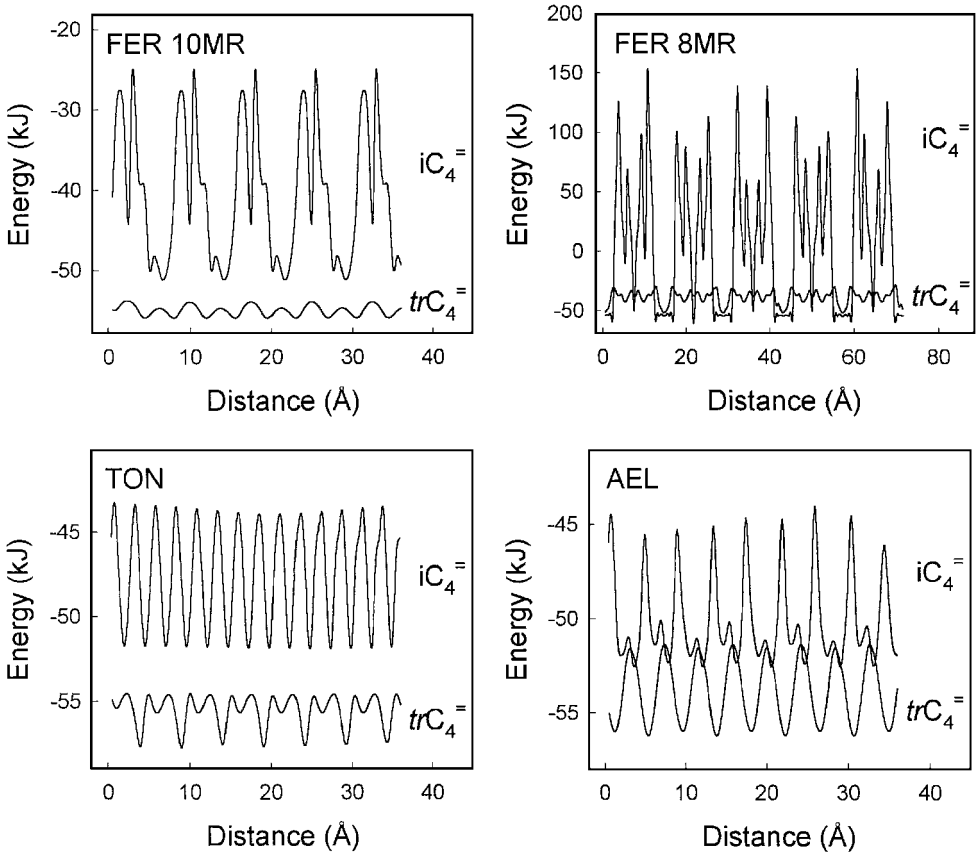

FIG. 11. Diffusion profile of isobutene ($iC_4^=$) and *tr*-2-butene ($trC_4^=$) in FER (along the 10 and the 8 MR channels) and TON and AEL (along the 10 MR channels).

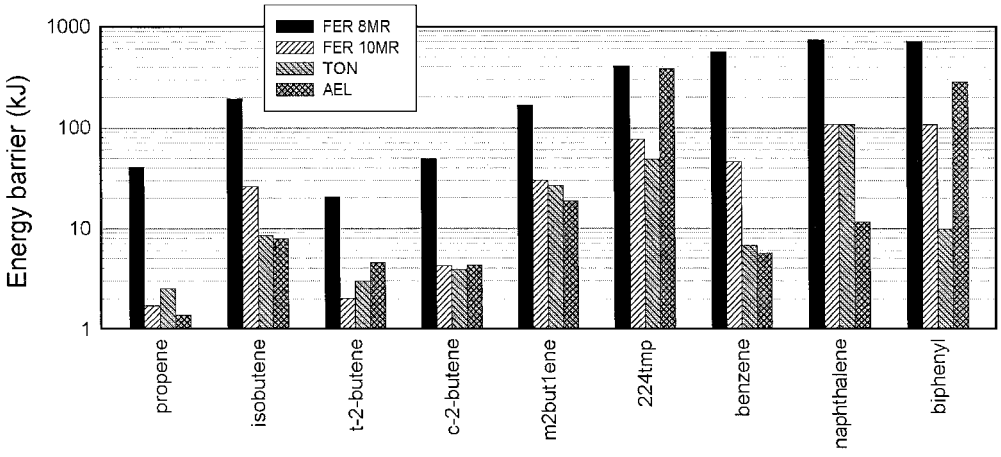

FIG. 12. Average energy barriers of various molecules in FER, TON, and AEL zeolites calculated from the periodic patterns of the diffusion profiles.

4. DISCUSSION

Evaluating the results of the current paper, one should keep in mind that these calculations do not give per se adsorption energies directly comparable to those experimentally measured. This is due to the fact that the molecular interactions are evaluated in this paper in an infinitely diluted adsorption state at zero Kelvin. Adsorption enthalpy (q_{st}) in theory equals an ensemble-averaged total energy of the adsorbate in the adsorbed state $\langle U_a \rangle$ and in ideal gas phase $\langle U_a \rangle_{IG}$ corrected with the temperature (20):

$$q_{st} = \langle U_a \rangle - \langle U_a \rangle_{IG} - k_B T.$$

However, the force field used here is "tuned" to give energies resembling the experimental values of heat of adsorption measured at moderate temperatures (27).

Indeed, the results obtained by molecular mechanics and dynamics calculations correlate well with experimental data due to this refined force field suited for zeolite applications. In our case, the potential energy for linear guest molecules in FER and TON match well with the adsorption data available on these zeolites (Fig. 6 and Ref. (24)). With increasing carbon number, comparable increments were found in the 10 MR channels of FER and TON.

A smaller increase in the potential energy was found in the case of the 8 MR channels in FER. This can be attributed to the more confined space in these pores, which has a twofold effect. With small molecules, the potential energy is enhanced, because the higher attractive forces allow stronger host–guest interactions with the more curved surface. With increasing chain length, however, the increased packing in the small volume of the 8 MR cages induces repulsive interactions, which dampen the increase in the total potential energy.

In contrast to the 8 MR terminated cages in FER, the elliptical channels of AEL allow a higher increase in the potential energy with increasing carbon number without the spatial restriction of the cagelike structure. Larger attractive forces are present during docking a guest in AEL; i.e., more oxygen atoms can have a close interaction with the hydrocarbon molecule in the elliptical pores without causing repulsion (Fig. 13). This higher interaction, therefore, will result in a larger increase in potential energy with increasing carbon number compared with FER.

Energies compiled here for C_4 isomers are in good agreement with those found in the literature using similar methods (25). The small differences might be due to the subtle differences in calculation methods, e.g., the representation of the zeolite structure.

4.1. Intermediates in the Bimolecular Mechanism

Three mechanisms have been proposed for describing the skeletal isomerization reaction of *n*-butenes (2–10). Much effort has been taken to justify the monomolecular mechanism (by using various quantum mechanical studies), in which the transition state is suggested to exhibit high potential energies and, therefore, might not be favored at reaction temperatures (2–4).

The bi- and pseudomonomolecular mechanisms do not involve such unique intermediates (5–9). Since the intermediates in these mechanisms are rather bulky (5, 8), they were not targeted in computational studies using quantum mechanics. Based on adsorption studies, it was speculated that the formation of the branched C_8 isomers is not favored in FER, since they cannot enter the pores (30). Furthermore, the cracking product distribution of C_8 olefins could not be matched with the original reaction pattern observed during *n*-butene isomerization. Note that (as argued before) C_8 molecules cannot enter the pores, and, therefore, are cracked at the outer surface of the zeolite particles (30). Despite the fact that in FER cages with inner diameters larger than the 10 or 8 MR openings exist, arguments

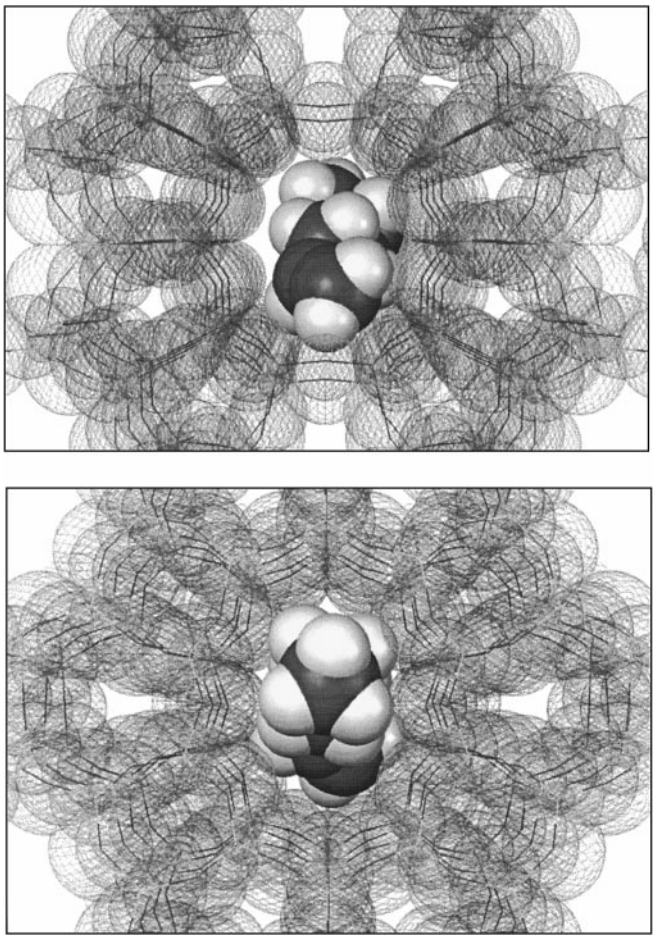

FIG. 13. Graphical representation of hex-1-ene in FER (top) and in AEL (bottom). Guest molecule is shown in CPK volume; zeolite, as a mesh model.

revoking that the formation of butene dimers is restricted inside the zeolite pores are frequently used in studies to conclude that the selective reaction leading to isobutene formation can be performed only *via* a monomolecular pathway (31–33).

The present calculations, however, entirely reconfirmed the proposal of Mooiweer *et al.* (5) that bulky C_8 molecules can be formed inside of FER, but they hardly can diffuse out of the pores. The calculated potential energies for all C_8 isomers were negative in every zeolite, and they were larger in numbers than what was obtained for C_6–C_7 linear olefins in the same frameworks. This justifies the energies obtained for the C_8 isomers in terms of calculating procedure, use of force field, and representation of the zeolites.

It is interesting to note that at first sight these results are inconsistent with those of obtained by van Well *et al.* (21, 22) based on adsorption studies and simulations using the configurational-bias Monte-Carlo (CB-MC) technique. However, it is worth pointing out that their simulations predicted that the higher linear isomers will not adsorb in the 8 MR pores of FER (22), contrary to their sorption experiments (21). This suggests that the CB-MC method using an approximation of the methyl and methylene groups with pseudoatoms is less suitable for confined spaces, where adsorption would be predicted by a simulation approach based on chemically more detailed models. Note that the CB-MC model successfully describes vapor–liquid phase equilibrias of linear alkanes over a large temperature range, where these constraints are virtually eliminated, and the use of large number of molecules is essential (34).

In branched molecules, the intramolecular interactions of methyl and methylene groups combined with the intermolecular interaction with the structured pore wall requires a chemically detailed description of the molecular structures, which is largely approximated in the CB-MC method due to the use of pseudoatoms. Our calculations, in contrast to the CB-MC predictions, indicate that branched C_8 molecules can be fitted into the 8 MR cavities of FER, with intimate interactions between the adsorbate molecule and the oxygen atoms in the pore wall.

Based on the high energy barriers obtained from diffusion pathway calculations, the results obtained suggest that the transport of the branched octanes is highly hindered in FER. This in good agreement with experimental findings (30) and previous calculations (5). Since similar barriers were found in TON and AEL (Fig. 12), hindered transport of bulky C_8 molecules is expected to occur in both zeolites. Note that the calculations clearly demonstrate that high stabilization can be achieved for branched octanes in FER, TON, and AEL at specific locations inside the framework, making the existence of such molecules in medium-pore zeolites viable.

Cracking of C_8 molecules can lead to various products (6). The intrinsic selectivity to isobutene during cracking is governed by the skeleton of the isomer and the location of the charge in the carbenium ion during transition state. Theoretically, a maximum number of isobutene molecules (N_{max}) per C_8 isomer can be derived for each different skeleton.

Accordingly, if this number (N_{max}) is equal to zero, no isobutene is obtained after cracking. If it is between 0 and 1, it means that cracking yields partially two C_4 skeletons (one of them is iC_4), and partially a pair of C_3–C_5, or others. When the number is equal to 1, after cracking a pair of iC_4 and nC_4 skeletons is obtained. This statistical number is plotted against the obtained potential energy for all the C_8 isomers in different zeolites in Fig. 14.

In general, with increasing numbers of iC_4 obtainable from a C_8 isomer a lower stabilization is calculated. For intrinsically nonselective C_8 isomers, FER, TON, and AEL showed similar stabilization energies. The selective C_8 isomers were, however, more stabilized in FER and AEL zeolites compared with TON. This let us speculate that the higher overall selectivity to isobutene might be related to

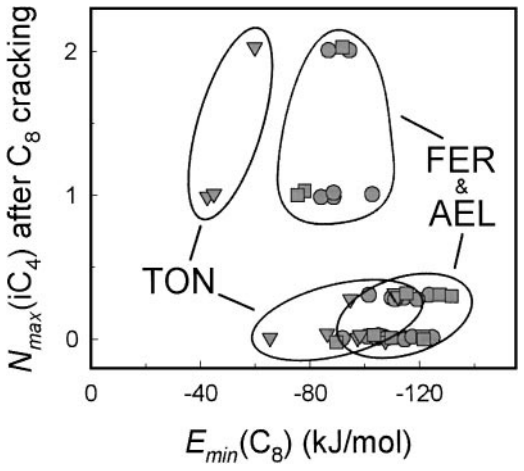

FIG. 14. Maximum number of isobutene molecules after cracking of a C_8 isomer (N_{max} vs the minimized potential energy of the corresponding C_8 isomer) in FER (circle), TON (triangle), and AEL (square) zeolites.

the stabilization of the particular C_8 isomers. Assuming an indirect effect, the population of the C_8 isomers is more favorable in FER and AEL in terms of selectivity to iC_4 cracking, while in TON it is governed mostly by unselective isomers.

To evaluate the absolute effect of such stabilization, the following arguments have to be taken into account simultaneously. (i) The thermodynamic equilibrium is pointing toward the very selective 2,2,4-trimethylpentane-derived skeleton. With significantly increased residence time, due to hindered diffusion, it is plausible to assume a good convergence to an equilibrium distribution. (ii) The stabilization provided by the host–guest interaction in the zeolite may affect the equilibrium population of C_8 isomers. Note that the smaller gap in energy between the less branched and less selective C_8 isomers and the more selective isomers with higher N_{max} in FER and AEL can induce a higher population of the more selective isomers in FER and AEL. (iii) The reactivity of the less selective isomers is higher due to the faster cracking reaction classified as type A cracking according to Guisnet *et al.* (6). We like to speculate that the extensive stabilization might outweigh the lower reactivity of the selective C_8 isomer resulting in a higher apparent activity toward the selective cracking in all catalysts, especially in FER and AEL.

4.2. Intermediates in the Pseudomonomolecular Mechanism

In the pseudomonomolecular mechanism an aromatic molecule is described as the selective catalytic site (10); it is a bulkier molecule compared with the C_8 olefins. In addition, it has been proposed that condensed aromatic structures, such as (substituted) naphthalenes, anthracenes, and phenanthrenes, are readily formed inside the pores of FER (6, 8), and can be recovered by careful decomposition of the zeolite framework (10).

Our calculations show that benzene and 1,2-biphenylethane can be stabilized in the pores, although they gained significantly less stabilization energy compared with alkanes and alkenes. These findings are in excellent agreement with experimental data, where either condensed polyenes or other noncondensed aromatic structures (35) were proposed based on *in situ* spectroscopic results.

Condensed structures, such as naphthalenes, however, are unlikely to be formed inside the channels of a 10 MR zeolite due to the very high repulsion caused by significant overlapping of the hydrogens in the aromatic rings and the oxygens in the wall of the pore (Fig. 15).

It is important to note that the rigidity of a hydrocarbon skeleton consisting of condensed rings does not allow significant torsion of the molecule. Because of the distance between the guest and host structures, the steric repulsion is hard to overcome by additional interaction with the pore wall initiating larger contribution of attractive forces and, thus, reducing the potential energy of the molecule. Note that the minimal geometric cross section of the naphthalene is considerably larger compared with that of a benzene ring due to the axial hydrogens.

Allowing the relaxation of the host structures in the close vicinity of the naphthalene molecules did not bring satisfactory compensation in the overall energy. A maximum reduction of 50 kJ/mol could be achieved by this method in FER. In TON and AEL, smaller decreases in the total energy were obtained. It is important to note that the cff91_czeo force field used here is not optimized on the positive side of the potential curve as much as it is fitted to the experimental values on the negative region of interactions.

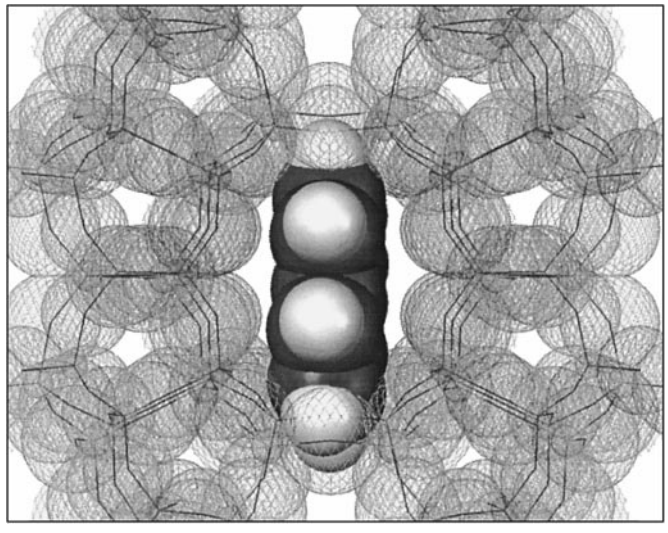

FIG. 15. Graphical representation of naphthalene in the 10 MR channels of FER. Guest molecule is shown in CPK volume; the zeolite, as a mesh model.

Therefore the energy values obtained for naphthalene can be used only as a qualitative indication of large repulsion forces.

5. CONCLUSIONS

Molecular modeling calculations were performed on a wide variety of hydrocarbon molecules observed in skeletal isomerization of *n*-butenes over 10 MR zeolites, such as FER, TON, and AEL. Monte-Carlo docking combined with minimization methods and diffusion pathway calculations (using continuous minimization) were used to explore the minimal potential energies of certain molecules in the framework, as well as to define the energy barrier in the potential energy for a molecule passing through the pore structure of those frameworks.

The minimal potential energies obtained for linear olefins were in good agreement with those obtained from adsorption studies (24). The energies found for docking C_8 isomers into FER, TON, and AEL indicate that these molecules can be viably fitted into the pores. Analysis of the energies showed that molecules that can be potentially cracked into isobutene were better stabilized in FER and AEL, while the potentially nonselective C_8 isomers (producing products other than nC_4 or iC_4 molecules) were equally stabilized in TON, FER, and AEL zeolites.

Selected intermediates proposed to play a crucial role in the pseudomonomolecular mechanism were tested in FER, TON, and AEL. Benzene and other noncondensed aromatic structures could be located in the pores, although they gained significantly less stabilization due to their rigid skeleton. Condensed aromatic molecules, such as naphthalene could not be fitted into the frameworks without avoiding large repulsive forces. This let us conclude that the formation of such condensed molecules is not favored in 10 MR zeolites, and therefore, their potential role in skeletal isomerization has to be reassessed.

ACKNOWLEDGMENT

Financial support from NWO/STW (Project 349-3797) is gratefully acknowledged.

REFERENCES

1. van Santen, R. A., and de Gauw, F. J. M. M., *Stud. Surf. Sci. Catal.* **130**, 127 (2000).
2. Cheng, Z. X., and Ponec, V., *Catal. Lett.* **27**, 113 (1997).
3. Boronat, M., Viruela, P., and Corma, A., *J. Phys Chem*. **100**, 633 (1996).
4. Sie, T., *Ind. Eng. Chem. Res.* **31**, 1881 (1992).
5. Mooiweer, H. H., de Jong, K. P., Kraushaar-Czarnetzki, B., Stork, W. H. J., and Krutzen, B. C. H., *Stud. Surf. Sci. Catal.* **84**, 2327 (1994).
6. Guisnet, M., Andy, P., Gnep, N. S., Benazzi, E., and Travers, C., *J. Catal.* **158**, 551 (1995).
7. Guisnet, M., Andy, P., Gnep, N. S., Benazzi, E., and Travers, C., *Oil Gas Sci. Technol.* **54**, 23 (1999).
8. Guisnet, G., Andy, P., Gnep, N. S., Travers, C., and Benazzi, E., *J. Chem. Soc. Chem. Commun.* 1685 (1995).
9. Guisnet, M., Andy, P., Boucheffa, Y., Gnep, N. S., Travers, C., and Benazzi, E., *Catal. Lett.* **50**, 159 (1998).
10. Andy, P., Gnep, N. S., Guisnet, M., Benazzi, E., and Travers, C., *J. Catal.* **173**, 322 (1998).
11. Rigby, A. M., Kramer, G. J., and van Santen, R. A., *J. Catal.* **170**, 1 (1997).
12. Boronat, M., Viruela, V., and Corma, A., *J. Phys. Chem. A* **102**, 982 (1998).
13. Asensi, M. A., and Martínez, A., *Appl. Catal. A* **183**, 155 (1999).
14. Butler, A. C., and Nicolaides, C. P., *Catal. Today* **18**, 443 (1993).
15. Meriaudeau, P., and Naccache, C., *Adv. Catal.* **44**, 505 (2000).
16. Gielgens, L. H., Veenstra, I. H. E., Ponec, V., Haanepen, M. J., and Hooff, J. H. C., *Catal. Lett.* **32**, 195 (1995).
17. Domokos, L., Lefferts, L., Seshan, K., and Lercher, J. A., *J. Catal.* **197**, 68 (2001).
18. Domokos, L., Lefferts, L., Seshan, K., and Lercher, J. A., *J. Mol. Catal. A* **162**, 147 (2000).
19. Domokos, L., Lefferts, L., Seshan, K., and Lercher, J. A., Submitted for publication.
20. Smit, B., and Siepmann, J. I., *J. Phys. Chem*., **98**, 8442 (1994).
21. van Well, W. J. M., Cottin, X., de Haan, J. W., Smit, B., Nivarthy, G., Lercher, J. A., van Hooff, J. H. C., and van Santen, R. A., *J. Phys. Chem*. **102**, 3945 (1998).
22. van Well, W. J. M., Cottin, X., Smit, B., van Hooff, J. H. C., and van Santen, R. A., *J. Phys. Chem*. **102**, 3952 (1998).
23. Schenk, M., Smit, B., Vlugt, T. J. H., and Maesen T. L. M., *Angew. Chem. Int. Ed.* **40**, 736 (2001).
24. Eder, F., and Lercher, J. A., *Zeolites* **18**, 75 (1997).
25. Jousse, F., Leherte, L., and Vercauteren, D. P., *J. Mol. Catal.* **119**, 165 (1997).
26. Eder, F., and Lercher, J. A., *J. Phys. Chem*. **100**, 16460 (1996).
27. Software manual for InsightII and Cerius^2 program package, or www.msi.com.
28. Freeman, C. M., Catlow, C. R. A., Thomas, J. M., and Brode, S., *Chem. Phys. Lett.* **186**, 137 (1991).
29. van Daelen, M. A., Li, Y. S., Newsam, J. M., and van Santen, R. A., *Chem. Phys. Lett.* **226**, 100 (1994).
30. Houzvicka, J., Klik, R., Kubelkova, L., and Ponec, V., *Catal. Lett.* **43**, 7 (1997).
31. Houzvicka, J., and Ponec, V., *Ind. Eng. Chem. Res.* **36**, 1424 (1997).
32. Xu, W.-Q., Yin, Y.-G., Suib, S. L., and O'Young, C.-L., *J. Phys. Chem*. **99**, 758 (1995).
33. O'Young, C.-L., Pellet, R. J., Casey, D. G., Ugolini, J. R., and Sawicki, R. A., *J. Catal.* **151**, 467 (1995).
34. Siepmann, J. I., Karaborni, S., and Smit, B., *Nature*, 365 (1993).
35. Pazé, C., Sazak, B., Zecchina, A., and Dwyer, J., *J. Phys. Chem. B* **103**, 9978 (1999).